Electronic Supplementary Material (ESI) for Catalysis Science & Technology.

Supplementary Information

Nonoxidative coupling of ethane with gold loaded photocatalysts

Surya Pratap Singh,[a] Akira Yamamoto,[a,b] and Hisao Yoshida[a,b,*]

[a] Graduate School of Human and Environmental Studies, Kyoto University, Kyoto 606-8501, Japan.

[b] Elements Strategy Initiative for Catalysts and Batteries (ESICB), Kyoto University, Kyoto 615-8245, Japan

[*] Corresponding author: yoshida.hisao.2a@kyoto-u.ac.jp

1 Experimental

1.1 Experimental set-up

The schematic experimental set-up used in the reaction test of photocatalytic direct ethane conversion is shown in Figure S1. A flow reactor similar to our previous works[1,2] was used in this study.

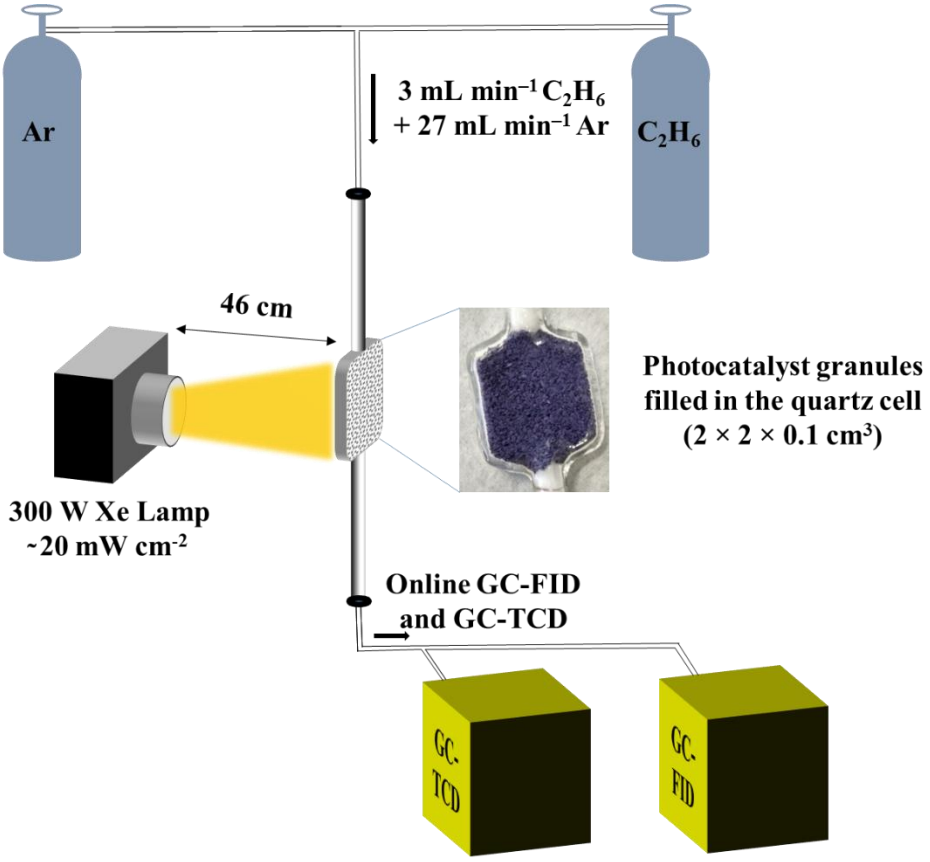

Figure S1 The schematic diagram of the experimental set-up used in the reaction test of photocatalytic ethane conversion, which is similar to our previous work. Inset: the photograph of the quartz sample cell filled with the granules of the Au(0.4)/TiO_2 sample. The size of the sample cell was 2 × 2 × 0.1 cm^3.

1.2 Spectral output of the xenon lamp

The spectral output of the Xe-lamp is shown in Figure S2. The lamp emits continuous light in the wavelength range of 200–800 nm with varying photon output in agreement with the uncorrected Xe-lamp spectrum reported in literature.[3,4]

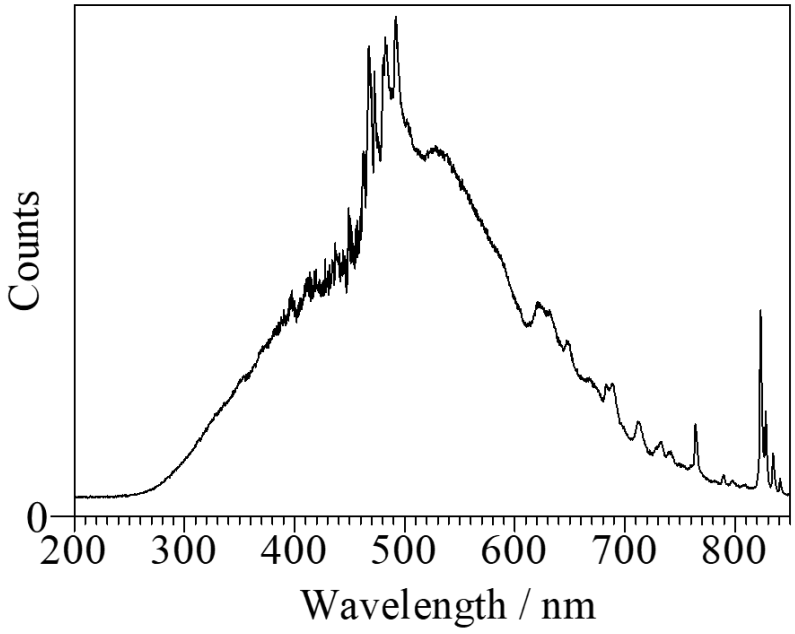

Figure S2 Spectral output of the Xe-lamp.

1.3 Calculations

1.3.1 Yield

The yield of hydrocarbons in the reaction is calculated based on the eq. 1, 2 and 5 in the main text as shown in eq. S1.

$$Yield\ (\%) = \frac{Consumption\ rate\ of\ ethane\ (2\times R_{C4H10}+R_{C2H4}+R_{CH4})}{Introduction\ rate\ of\ ethane} \times 100 \qquad \text{(S1)}$$

1.3.2 Selectivity

The product selectivity based on ethane toward *n*-butane and ethene are calculated as shown in eq. S2 and S3, respectively.

$$S_{C4H10}\ (\%) = \frac{2\times R_{C4H10}}{2\times R_{C4H10}+R_{C2H4}+R_{CH4}} \times 100 \qquad \text{(S2)}$$

$$S_{C2H4}\ (\%) = \frac{R_{C2H4}}{2\times R_{C4H10}+R_{C2H4}+R_{CH4}} \times 100 \qquad \text{(S3)}$$

1.3.3 *R* value

The ratio of the obtained hydrocarbons and hydrogen, $R_{HC/H2}$ is defined as follows (eq. S4).

$$R_{HC/H2} = \frac{R_{C4H10}+R_{C2H4}-R_{CH4}}{R_{H2}} \qquad \text{(S4)}$$

where R_{C4H10}, R_{C2H4}, R_{CH4}, and R_{H2} are the production rates of *n*-butane, ethene, methane, and hydrogen, respectively.

1.3.4 Apparent quantum efficiency (AQE)

The apparent quantum efficiency (AQE) was calculated by the following equation as the ratio of the number of consumed holes for the n-butane formation (or ethene formation) and the number of incident photons.[5]

$$AQE\ (\%) = \frac{r\times n\times N}{(I\times A)/(hc/\lambda)} \times 100 \qquad \text{(S5)}$$

where r = production rate of C_4H_{10} (or C_2H_4) (in mol s^{-1}), n = number of holes consumed for the production of C_4H_{10} (or C_2H_4) (n=2), N = Avogadro constant (in mol^{-1}), I = intensity of the incident light estimated in the wavelength range of 200–420 nm (from the measured value in the wavelength range of 220–300 nm by a UV radiometer and the DR UV-vis absorption spectrum)

(in W cm^{-2}), A = Area of the reactor (in cm^2), h = Planck's constant (in J s), c = speed of light (in m s^{-1}), λ = wavelength of incident light (in m).

2 Results and discussion

2.1 GC-TCD and GC-FID chromatograms

The chromatograms of the GC-TCD and the GC-FID after 1.5 h of the photocatalytic reaction test over the Au(0.4)/TiO_2 sample are shown in Figure S3 and Figure S4, respectively.

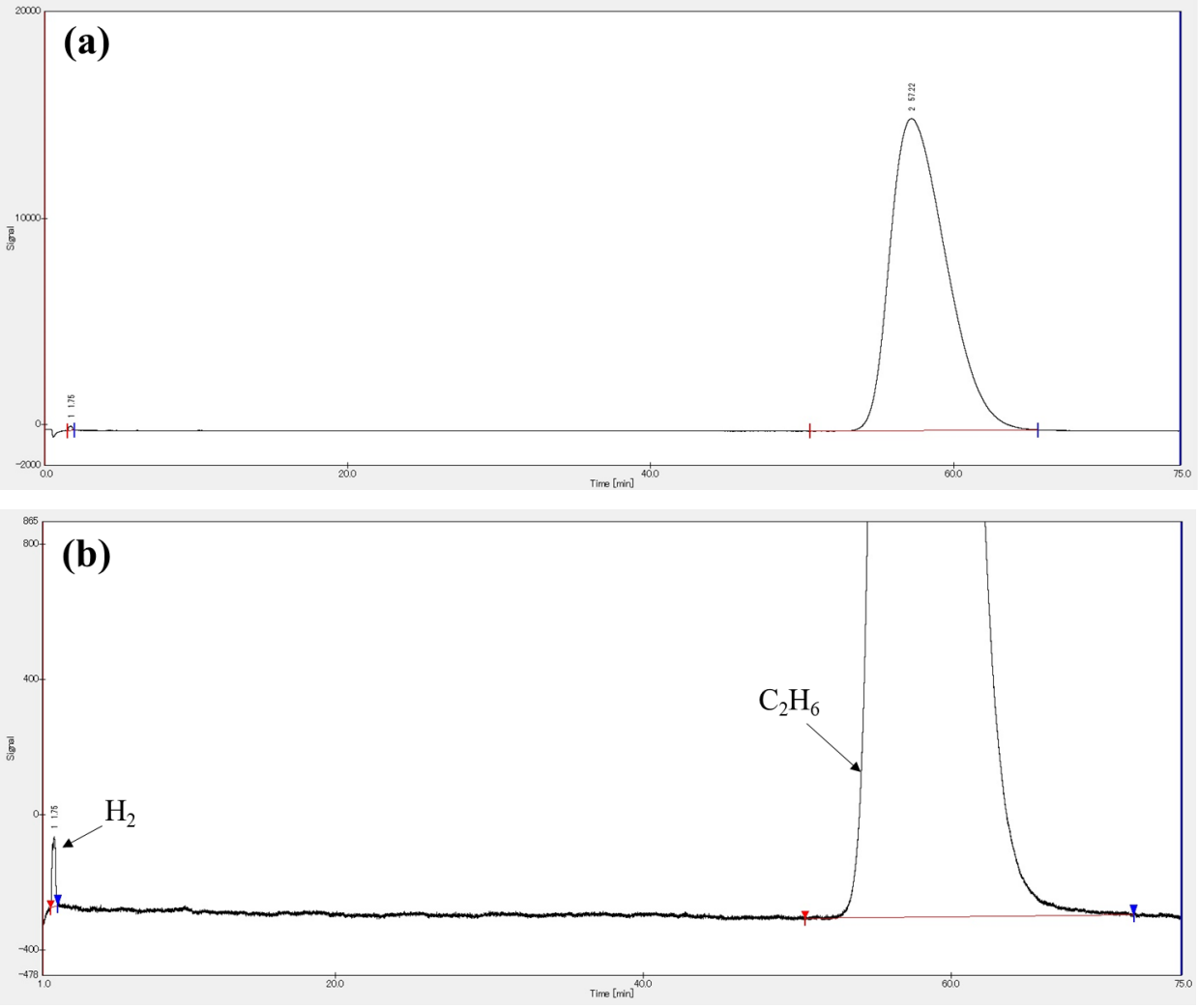

Figure S3 GC-TCD chromatograms, (a) original and (b) magnified, after 1.5 h of the reaction test of photocatalytic direct ethane conversion over the Au(0.4)/TiO_2 sample. GC-TCD was used to analyze mainly hydrogen. The peaks of hydrogen (retention time = 1.7 min) and ethane (57 min) can be seen distinctively and were well separated.

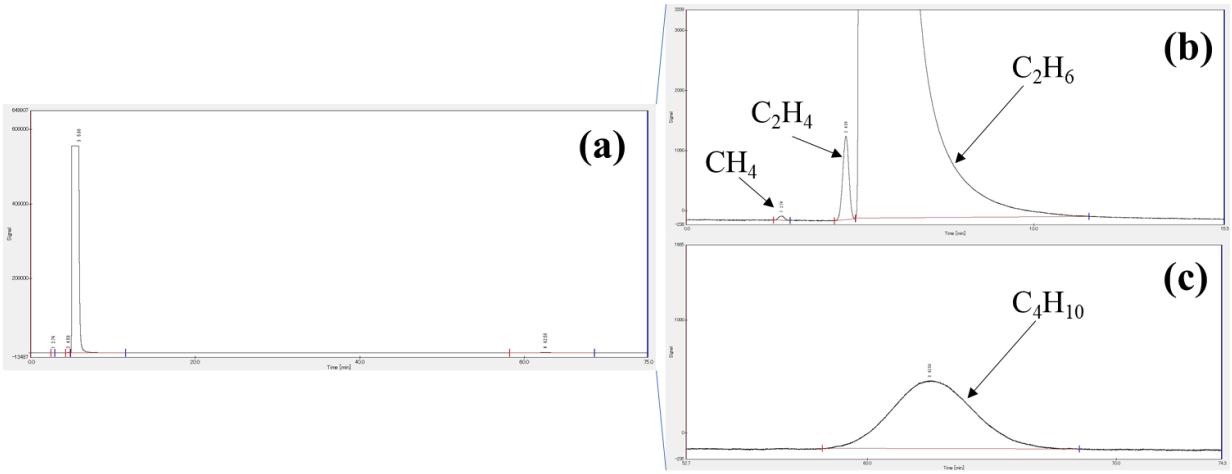

Figure S4 GC-FID chromatogram, (a) original and (b-c) magnified, after 1.5 h of the reaction test of photocatalytic direct ethane conversion over the Au(0.4)/TiO_2 sample. The GC-FID was used to analyze mainly the hydrocarbons. The peaks of methane (2.8 min), ethene (4.6 min), ethane (5.9 min), and *n*-butane (62 min) can be seen distinctively and were well separated. No *i*-butane (48 min) was detected.

2.2 DR UV-vis spectrum of Al_2O_3

The DR UV-vis spectrum of the bare Al_2O_3 sample is shown in Figure S5. A small absorption was observed in the wavelength range of 200–350 nm.

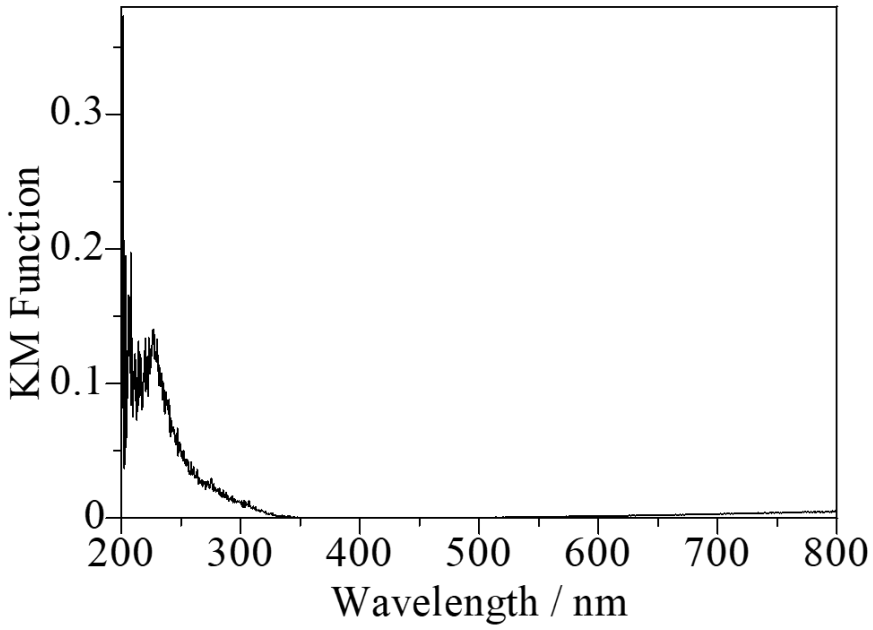

Figure S5 DR UV-vis spectra of the bare Al_2O_3 sample.

2.3 Estimation of loading amount of Au in the Au(*x*)/TiO_2 samples

The actual loading amounts of Au determined by the XRF analysis in various Au(*x*)/TiO_2 samples are given in Table S1.

Table S1 Loading amount of Au in Au(*x*)/TiO_2 samples

S. No.	Sample [a]	Loading amount of Au (mol %) [b]
1	Au(0.1)/TiO_2	0.08
2	Au(0.2)/TiO_2	0.18
3	Au(0.4)/TiO_2	0.42
4	Au(1.0)/TiO_2	1.04

[a] The samples were prepared by the photodeposition method. [b] Determined by XRF.

2.4 XRD patterns of Au/TiO_2 samples

XRD patterns of the TiO_2 and various Au/TiO_2 samples are shown in Figure S6. The lines derived from Au nanoparticles were evident for the $Au(1.0)/TiO_2$ sample.

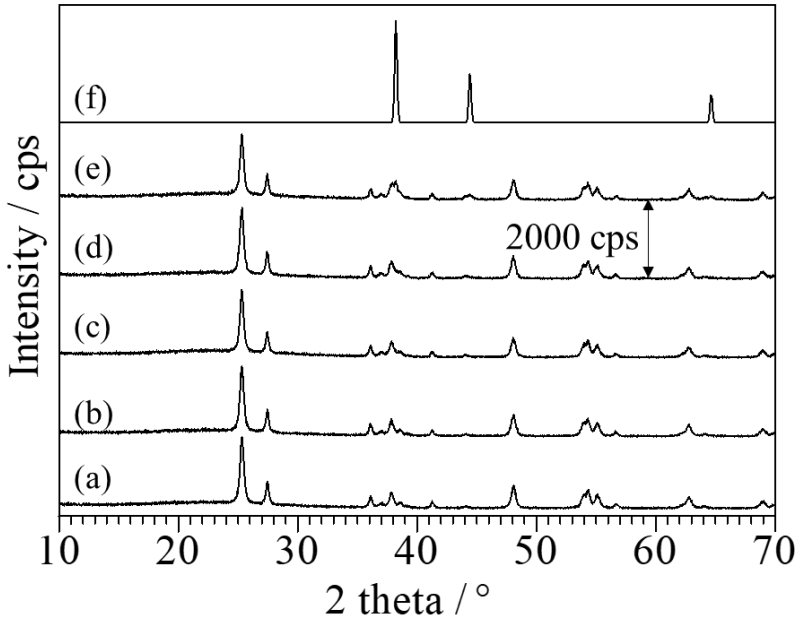

Figure S6 XRD patterns of the samples, (a) TiO_2, (b) $Au(0.1)/TiO_2$, (c) $Au(0.2)/TiO_2$, (d) $Au(0.4)/TiO_2$, (e) $Au(1.0)/TiO_2$, and (f) Au from the database (ICSD#52249).

2.5 SEM images and EDX elemental mappings

Figure S7 shows SEM images and elemental mappings. In the TiO_2 sample, no regular shape of TiO_2 particles could be seen and the agglomeration of nanoparticles was observed (Figure S7a). In the Au(0.4)/TiO_2 sample, the morphology did not change much and the Au nanoparticles were dispersed on the TiO_2 surface (Figure S7 b-e).

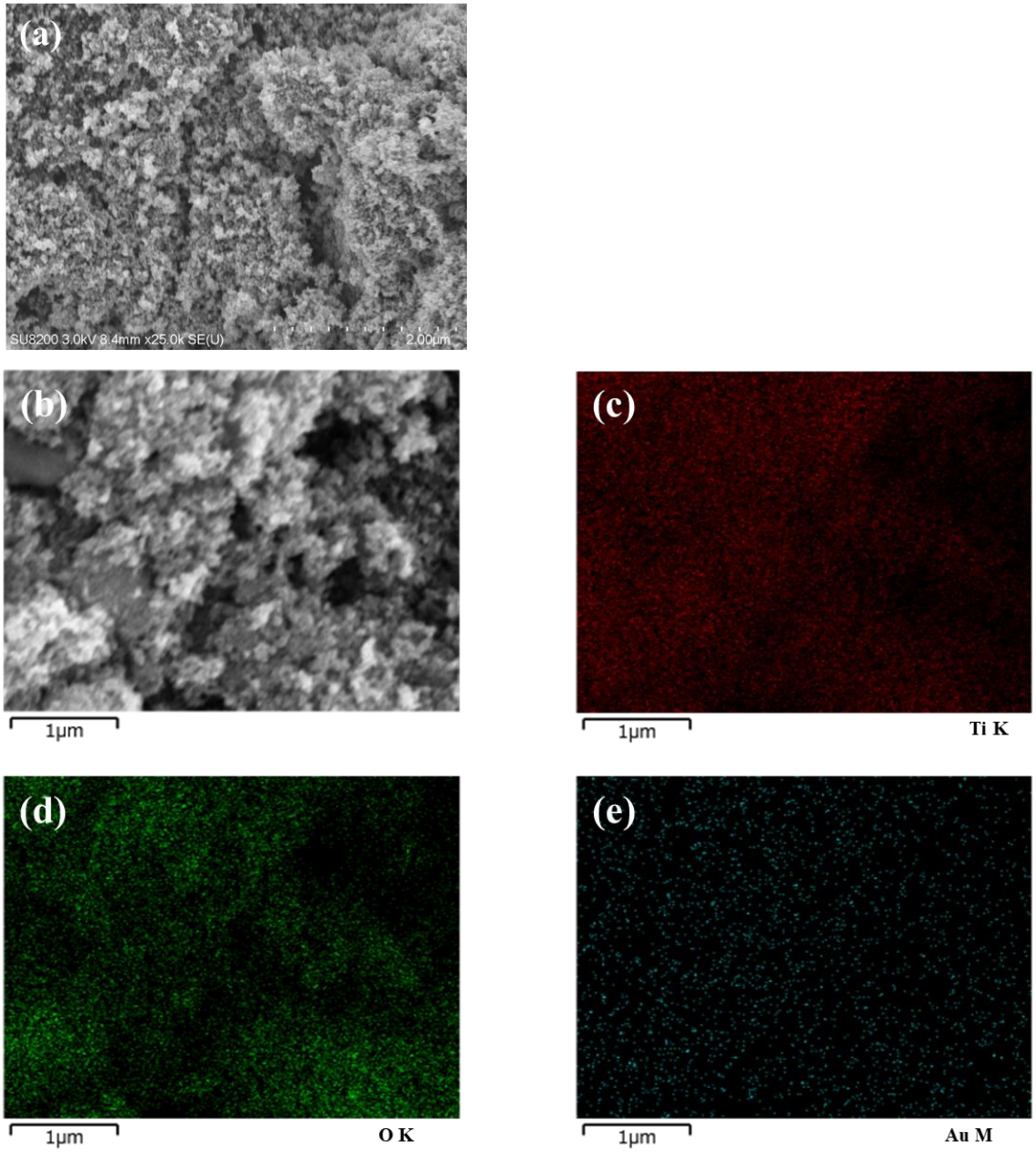

Figure S7 (a) SEM image of the bare TiO_2 sample, and (b) the SEM image and (c-e) elemental mappings of the Au(0.4)/TiO_2 sample.

2.6 STEM images and particle size distribution of Au nanoparticles in the Au/TiO_2 samples

The STEM images and the particle size distribution of Au nanoparticles in the Au(0.1)/TiO_2, Au(0.2)/TiO_2, and Au(1.0)/TiO_2 samples are shown in Figure S8. With an increase in the loading amount of Au, the particle size of Au nanoparticles is increased in the Au/TiO_2 samples.

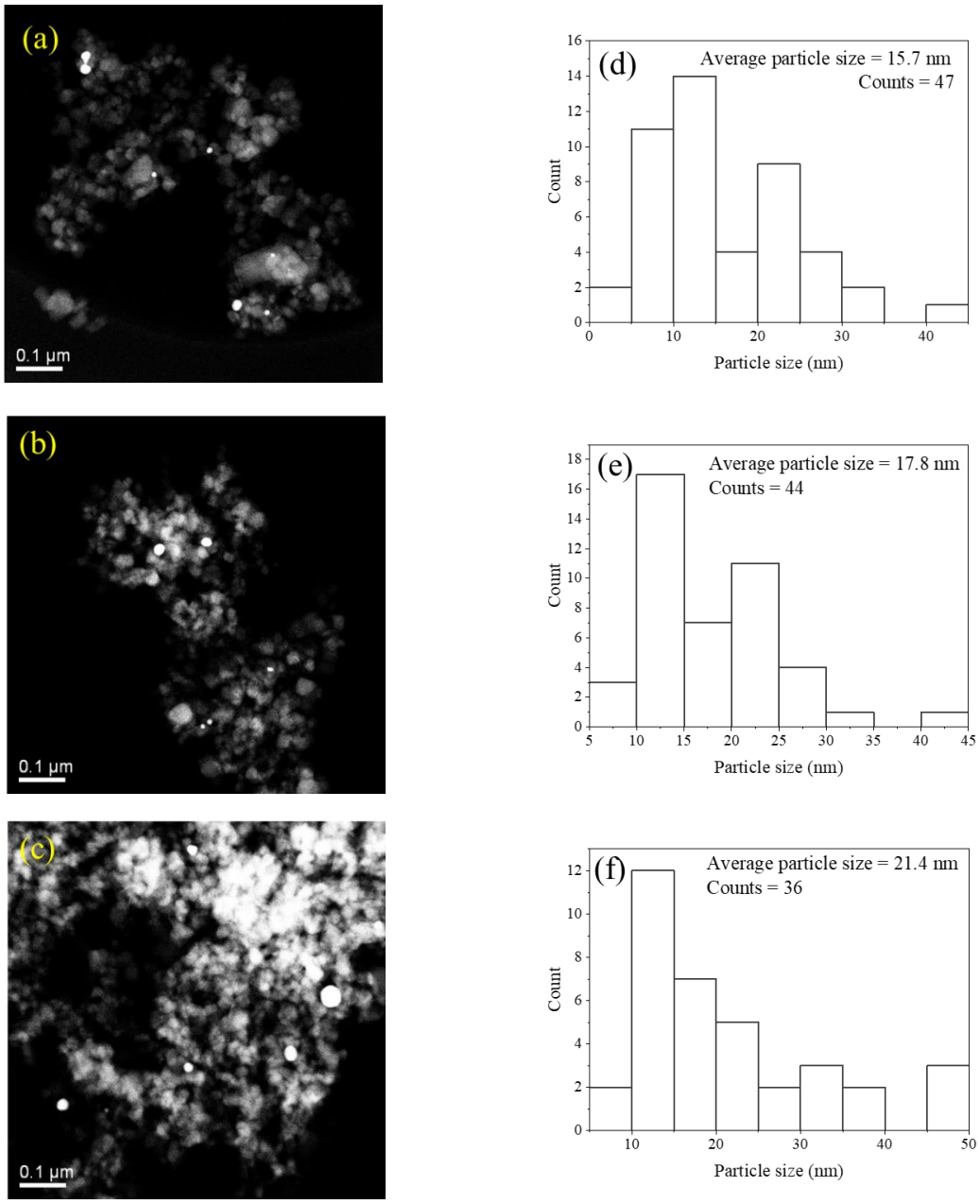

Figure S8 STEM images (a–c) and particle size distribution of Au nanoparticles (d–f) in the Au(0.1)/TiO_2, Au(0.2)/TiO_2, and Au(1.0)/TiO_2 samples.

2.7 DR UV-vis spectra of Au/TiO_2 samples

The DR UV-vis spectra of various Au/TiO_2 samples are shown in Figure S9. An additional broad band cantered at 550 nm due to the LSPR of Au nanoparticles was observed in the DR UV-vis spectra of the Au/TiO_2 samples. The intensity of this band increased with an increase in the loading amount of Au, where a slight red shift was observed.

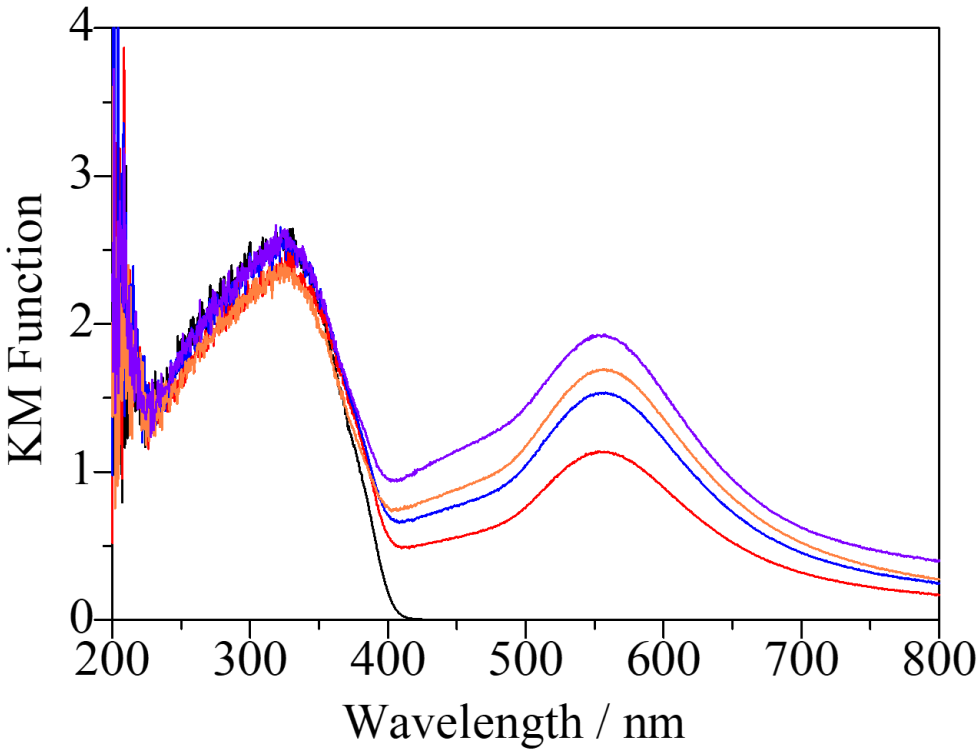

Figure S9 DR UV-vis spectra of the samples; TiO_2 (black line), $Au(0.1)/TiO_2$ (red line), $Au(0.2)/TiO_2$ (blue line), $Au(0.4)/TiO_2$ (orange line), and $Au(1.0)/TiO_2$ (violet line).

2.8 Effect of thermal energy in the dark

Catalytic reaction tests in dark at various temperatures were carried out with the Au(0.4)/TiO_2 and Au(0.4)/Ga_2O_3 samples and the results are given in Table S2 and Table S3, respectively.

Table S2 Effect of increasing the temperature in dark with the Au(0.4)/TiO_2 sample[a]

Entry	Temperature	Production rates[b] / μmol h^{-1}				
	(K)	C_4H_{10}	C_2H_4	CH_4	C_3H_6	H_2
1	323	nd[c]	nd[c]	nd[c]	nd[c]	nd[c]
2	373	nd[c]	nd[c]	nd[c]	nd[c]	nd[c]
3	423	nd[c]	nd[c]	nd[c]	nd[c]	nd[c]
4	473	nd[c]	nd[c]	nd[c]	nd[c]	nd[c]
5	523	nd[c]	0.026	0.22	nd[c]	0.48
6	573[d]	nd[c]	0.025	0.28	trace[e]	1.1
7	623 [d]	nd[c]	0.23	0.27	trace[e]	1.9
8	673 [d]	nd[c]	3.3	0.38	trace[e]	7.1
9	723 [d]	nd[c]	23.5	0.82	trace[e]	31.2

[a]Other reaction conditions were same as those described in the footnote *a* of Table 1 in the main text. [b]Production rates were measured after 1.5 h at each temperature. [c]nd = not detected. [d]Small amount of CO was also observed. [e]The amount of the product was less than 0.01 μmol h^{-1}.

Table S3 Effect of increasing the temperature in dark with the Au(0.4)/Ga_2O_3 sample[a]

Entry	Temperature	Production rates[b] / μmol h^{-1}				
	(K)	C_4H_{10}	C_2H_4	CH_4	C_3H_6	H_2
1	323	nd[c]	nd[c]	nd[c]	nd[c]	nd[c]
2	373	nd[c]	nd[c]	nd[c]	nd[c]	nd[c]
3	423	nd[c]	nd[c]	nd[c]	nd[c]	nd[c]
4	473	nd[c]	nd[c]	nd[c]	nd[c]	nd[c]
5	523	nd[c]	trace[d]	0.07	nd[c]	0.17
6	623[e]	nd[c]	8.4	0.10	trace[d]	10.2
7	673[e]	nd[c]	126.2	0.11	trace[d]	128.8

[a]Other reaction conditions were same as those described in the footnote *a* of Table 1 in the main text. [b]Production rates were measured after 1.5 h at each temperature. [c]nd = not detected. [d]The amount of the product was less than 0.01 μmol h^{-1}. [e]Small amount of CO was also observed.

References

1 S. P. Singh, A. Anzai, S. Kawaharasaki, A. Yamamoto and H. Yoshida, *Catal. Today*, 2021, **375**, 264–272.

2 S. P. Singh, A. Yamamoto, E. Fudo, A. Tanaka, H. Kominami and H. Yoshida, *ACS Catal.*, 2021, **11**, 13768–13781.

3 S. Rolt, P. Clark, J. Schmoll and B. J. R. Shaw, *Sp. Telesc. Instrum. 2016 Opt. Infrared, Millim. Wave*, 2016, **9904**, 99044V.

4 Y. Lu, Z. Shen and Y. Zhou, *J. Opt. Technol.*, 2013, **80**, 474.

5 M. Ishimaru, F. Amano, C. Akamoto and S. Yamazoe, *J. Catal.*, 2021, **397**, 192–200.